CHAPTER 4

A. Experimental and Theoretical Revelation of a Unique Band Topology in Sb_2Te_3 Topological Insulator by Substitution of Cu- A High Pressure Study

4.A.1 Introduction

Topological Insulators (TIs) are novel states of quantum matter[15], [182]. TIs host insulating bulk and spin-dependent, time-reversal symmetry protected conducting surface states due to strong spin orbit coupling (SOC). The three-dimensional (3D) TIs have been extensively studied in the recent years due to their electronic topological transition (ETT)[183]–[185], structural[107], [186], metal-insulator transition[187], [188] and potential applications for superconductivity[106], [189], [190]. The ETT[191], [192] has been widely studied as it helps to understand the topological changes near the Fermi surface. It is defined as a 2.5 order transition in the Ehrnfrest classification scheme and does not involve a volume discontinuity similar to second order structural transitions. However, changes in elastic constants and compressibility are significant. ETT can be observed by changes in Raman line width (FWHM) of vibrational modes, bulk modulus and ratio of c/a in hexagonal crystal lattice[185], [193].

Topological Insulating materials with A_2B_3 type of structure have been widely nurtured with a primary focus of understanding and identifying the ETT[194]–[196]. ETT has been mainly detected in pristine Sb_2Te_3, Bi_2Te_3 and Bi_2Se_3 compounds at around 3-5 GPa [183]–[185]. It has been observed that doping reduces the pressure of the ETT in TIs. Doping affects the ETT transition pressure substantially due to electronic structure of the dopant and its interaction with the host element. In crystal systems, doping can act as an internal pressure agent[197]–[199] which may affect the band structure as a result of electronic overlap. A pronounced anomaly near 2.8 GPa was detected and identified as a signature of ETT in $AgBiSe_2$ [200]. Similarly, in Bi doped Sb_2Te_3[201], softening of Raman mode along with thermoelectric maxima at 1.7 GPa under hydrostatic condition was observed. Kang group[202] also established linewidth anomaly along with c/a abnormal changes at 3 GPa in Se doped Bi_2Te_3 compound. Chao et al.[203] distinguished an insulator to metal

transition instead of an ETT at 9 GPa due to closure of bulk band gap in Sn-doped $Bi_{1.1}Sb_{0.9}Te_2S$. A recent report on layered compound MoSSe revealed a new electronic transition near 3 GPa which was not observed even in the parent compounds MoS_2 or $MoSe_2$ [204].

Furthermore, the phenomenon of metallization under pressure is very interesting and can be used as the basis of pressure conducting (insulating) switches and sensors[205], [206]. It is interesting to note that in this family of compounds, the pressure induced semiconductor to metallic transition has not been uniformly observed by all researchers. For example, in TI Sb_2Te_3, it was observed in theoretical DFT calculation[207], but experimentally some studies reported it while others did not[189], [208]. The analogues transition was found to be absent in theoretical prediction of Bi_2Te_3[190] while experimentally a semiconductor to metal transition was achieved in the same material[187], [209]. The report by Zhang et al.[188] revealed metallization of Bi_2Se_3 above 9.7 GPa. However, the theoretical DFT calculation on Bi_2Se_3[210] was unable to assign this transition. Hence the present study was undertaken to further understand this transition.

In literature it has been shown that copper doping tunes the electronic structure and has led to the enhancement /occurrence of topological superconductivity at room pressure [106], [197], [211]–[213]. Cu was found to act as an ambipolar atom in Bi_2Se_3[214], [215]; besides, Cu is capable of shifting and changing the shape of bands near the Fermi surface[216]. In the present study, we report high pressure Raman and x-ray diffraction studies on Cu doped Sb_2Te_3. The intriguing feature of this investigation is the presence of two electronic transitions (a semiconductor to metal transition along with an ETT) due to closure of bulk band gap and changes in topology of the Fermi surfaces respectively. Theoretical calculations were also performed to understand the experimental results.

4.A.2 Methods

4.A.2.1 Computational details

The theoretical calculations were performed using VASP (Vienna ab initio simulation package)[110] to probe the electronic properties of Cu-doped Sb_2Te_3 under pressure. The simulations use the GGA (generalized gradient approximation) of PBE (Perdew-Burke-Ernzerhof) exchange-correlation functional. A plane wave basis with a cutoff of 400 eV was used and SOC was included in all calculations. The Gaussian smearing method along with a smearing width equal to 0.10 eV was chosen for Brillouin zone integration. We followed the energy convergence limit up to 1×10^{-5} eV for all sets of calculations. To simulate the $Sb_{1.9}Cu_{0.1}Te_3$ a 2×2×1 supercell with 1 Cu atom out of total 60 atoms is constructed for the calculation[111]. Experimental lattice parameters and wycoff positions were used to perform the calculation. A K-mesh of 8×8×1 was generated for the SCF run followed by band structure and DOS calculations.

4.A.3 Results and discussion

4.A.3.1 XRD Pressure was increased in step of 1–2 GPa up to 32 GPa during in situ synchrotron x-ray diffraction measurement at ambient temperature. To acquire the cell parameters and atomic coordinates, Rietveld and Le Bail refinements were performed at various pressures using the GSAS + EXPGUI program. We observe that the modeled crystal structure of $Sb_{1.9}Cu_{0.1}Te_3$ sample crystallizes in a hexagonal structure with R-3m space group (phase-1, S.G.=166, Z=3, α-phase) according to the XRD pattern analysis at 0.3 GPa. The diffraction data of the material at different pressures and the Rietveld/ Le Bail refined patterns for the different high- pressure phases has been depicted in in Figure 4.A.1 (a-e).

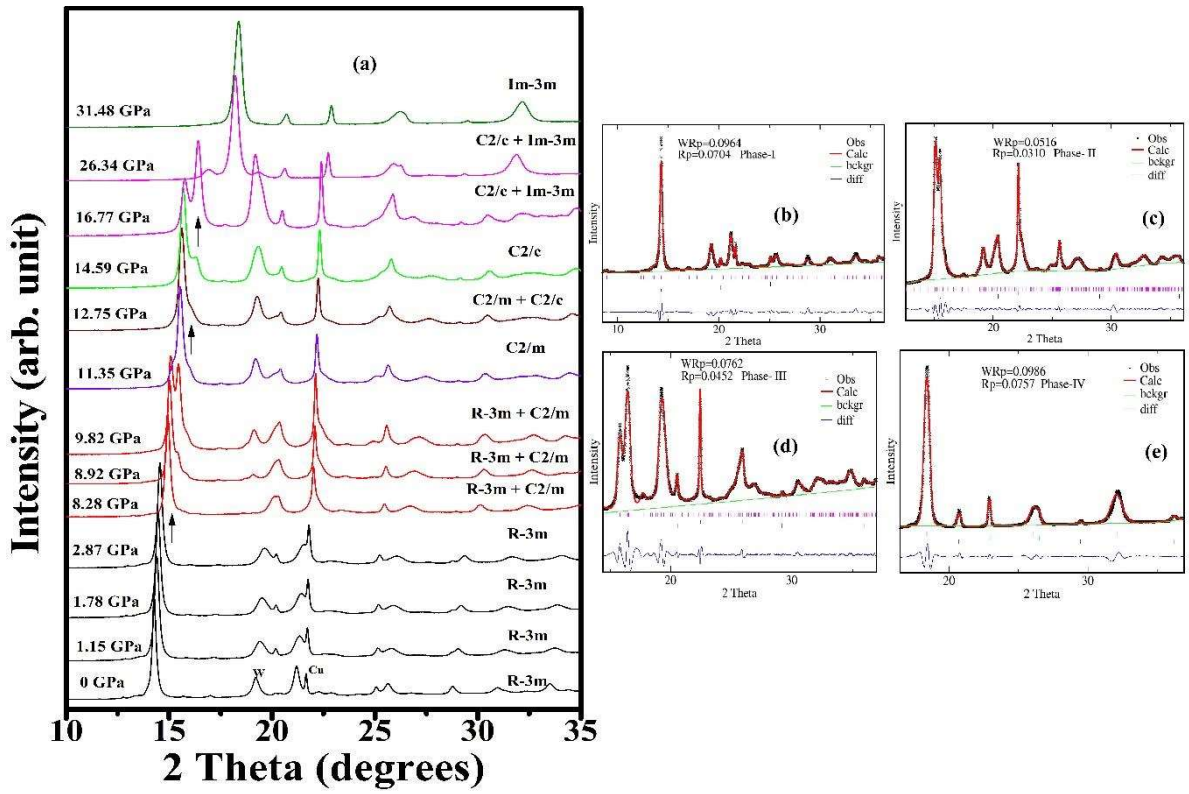

Figure 4.A.1 (a) ADXRD patterns collected at various pressures for $Sb_{1.9}Cu_{0.1}Te_3$. The new peaks are marked with arrows, for phases II (C2/m), III(C2/c), and IV(Im-3m), respectively, Rietveld full-profile refinements of the diffraction patterns collected on compression at (b) 0.26 GPa (Rhombohedral R-3m phase), Le-Bail refinements of the diffraction patterns (c) 9.8 GPa (Monoclinic C2/m phase) and (d) 16.77 GPa (Monoclinic C2/c phase) and (e) 31.48 GPa (disordered cubic Im-3m phase) the difference plot is given below. The difference plot is shown in blue. Background is shown as green and the vertical marks give the individual phases of sample, Cu and W.

The arrows at high pressure indicate the presence of new diffraction peaks heralding structural phase transitions in Fig. 4.A.1a. In our studies we observed three structural phase transitions. A monotonous shift was observed in the diffraction peaks upto 8 GPa. However, beyond that pressure we observe a subtle shoulder emerging around 2θ=15° (shown by arrow). The diffraction peaks of this new phase could be indexed with the C2/m phase (Phase-II, S.G.=12, Z=4, β phase) similar to[107], [217]. The phase II was initiated around 8 GPa and continues up to 12.75 GPa. Previous investigations on electrical resistivity and XRD reveals a structural transition at 8 GPa[218] or 7-10 GPa[196] in the

parent sample. For Bi_2Te_3, the initiation of the II phase was observed above 8.41 GPa[219]. The coexistence of these two phases was found up to 10.7 GPa in pristine Sb_2Te_3 [107].

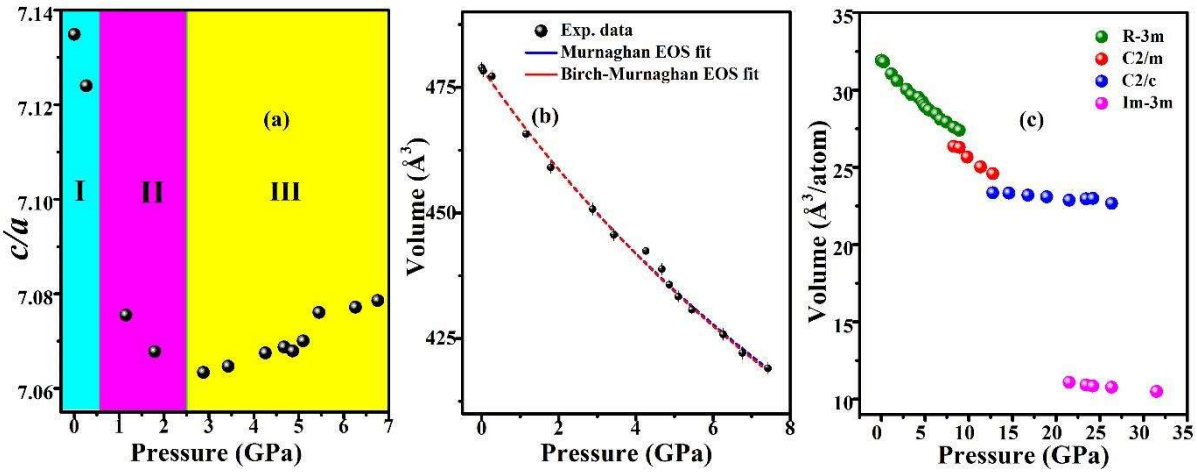

Figure 4.A.2 (a)c/a ratio as a function of pressure for ambient rhombohedral (R-3m) phase, 3 different colors indicate slope changes at those regions, (b) The volume as a function of pressure for initial rhombohedral phase with error bars. The dashed lines are the fitting results according to the third-order Birch-Murnaghan (red) and Murnaghan (blue) EoS, (c) Pressure dependence of the volume per atom (V/atom) for all the four phases.

A new diffraction peak (also shown by arrow) appeared at 2θ=16° when the pressure is above 11.35 GPa, becomes stronger in intensity with pressure. This indicates the presence of a second high pressure phase transition at this pressure. The third phase could be indexed to the C2/c phase (Phase-III, S.G.=15, Z=4, γ-phase) similar to what[107], [193].

The coexistence of two monoclinic phase C2/m and C2/c persists up to 12.75 GPa. According to earlier reports[107], [193] the co-existence of phase II and III continues in a pressure range 15.2 -19.2 GPa and 13.2-16.9 for Sb_2Te_3. However, Zhao et al showed that the third phase had a disordered C2/m structure[217]. On further increasing the pressure most of the diffraction peaks lose intensity above 16 GPa and the diffraction pattern could be indexed to a bcc Im-3m phase (Phase-IV, S.G.=229, Z=1, δ-phase). It was observed that above 31 GPa, $Sb_{1.9}Cu_{0.1}Te_3$ completely found to be converted into the Im-3m structure. In pure Sb_2Te_3 this transformation to a disordered cubic phase was observed at slightly lower

pressure of 29.7 GPa[217]. The coexistence of phase III and IV took place in a pressure range of 21.6-28.4 GPa [107] for pristine material.

Figure 4.A.2(a) shows the plot of c/a as a function of pressure. It was observed that the c/a ratio shows changes in its slope at ~1 GPa and 2.5 GPa which has been represented by different colours. Though it is difficult to assign subtle changes in the slope of the c/a ratio to a phase transition, observation of a minima at 2.5 GPa certainly supports the presence of an electronic topological transition. In fact earlier studies have assigned this minima to the

Table 4.A.1 Comparison of experimental ETT and structural transitions (GPa) observed in various TIs.

Materials	**ETT (GPa)**	**I → II (GPa)**	**II → III (GPa)**	**III → IV (GPa)**
Bi_2Te_3[222]		8	13	16
Bi_2Te_3[183]	4	7.4	15.5	21.6
Bi_2Te_3[186]		8	14	Above 14
Sb_2Te_3[186]		9	15	20
Sb_2Te_3[185]	3.5	7.7	14.5	25
Sb_2Te_3[193]	3.7	13.2	15.2-19.2	Above 19.2
Sb_2Te_3[207]	2, 4.25	-	-	-
Cu-Sb_2Te_3 [This work]	<1, 2.5	Above 8	12.75	16.77

presence of an ETT as well as a signature of an insulator to metal transition[203], [220], [221]. Comparison of experimental ETT and structural transitions observed in various materials of this family is listed in Table 1. From this table it is clear that the all the phase

transformation pressures are lowered in the doped Sb_2Te_3 when compared to the parent compound.

We have also fitted our P-V data with third order Murnaghan equation of state and the fitting yielded similar results to Birch–Murnaghan (BM EOS), shown in Figure 4.A.2(b). Lattice parameters and bulk modulus (obtained from BM EOS) for our experimental results of α-phase are compared with earlier published results and listed in **Table 4.A.2.**

***a*(Å)**	***c*(Å)**	***B*₀(GPa)**	***B*′₀**	**References**
4.275	30.400	40.6	5.1	[193]
4.262	30.450	40	4	[218]
4.265	30.450	30.2	9.4	[196]
4.263(53)	30.41(99)	42.57	3.83	**This Work**

Higher values of B_0' α-phase implies larger changes in volume compressibility under pressure[205]. This further implies that the exceptional compression may be the reason behind the multiple electronic transitions in phase I.

The volume per atom value for each phase is plotted in Figure 4.A.2(c). To have better understanding of any electronic transition, we fitted our experimental results with the Universal Equation of State (UEOS). The UEOS is proposed by Vinet and given by:

$$\boldsymbol{lnH_{VIN} = lnB_o + \eta(1 - X)} \qquad \textbf{(4.A.1)}$$

Where $\boldsymbol{H = PX^2/3(1 - X)}$ and $\boldsymbol{X = (V/Vo)^{1/3}}$, η being related to the pressure derivative (B'_o) of the bulk modulus B_o, $\boldsymbol{\eta = 3(B'_o - 1)/2}$ and V is the volume at pressure P and

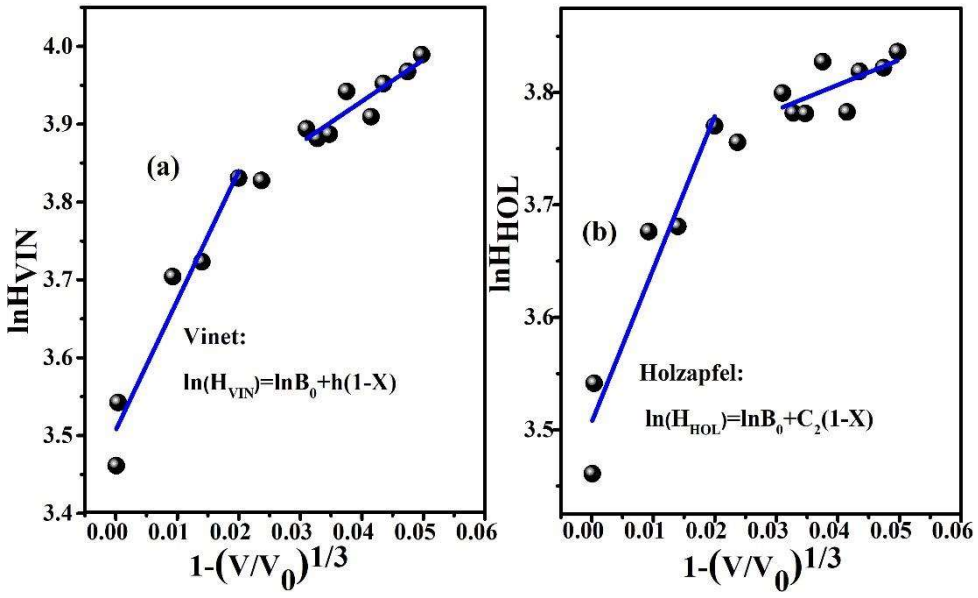

Figure 4.A.3 Fit of compressibility with universal equation of state; blue solid line is (a) fit with Vinet EOS, (b) fit with Holzapfel EOS.

V_0 is the ambient volume. The plotted curve is given is shown in Figure 4.A.3(a). The distinct slope change is attributed to the presence of electronic transition in the system. The UEOS, clearly shows deviation from linearity near V/V_0 =0.95. In order to assess the accuracy of our results we also fitted our data (shown in Figure 4.A.3b) with Holzapfel equation of state[223]:

$$\boldsymbol{lnH_{Hol} = \ln(B_o) + C_2(1 - X)} \qquad \textbf{(4.A.2)}$$

Where, $\boldsymbol{H_{Hol} = \frac{PX^5}{3(1-X)}}$ and $\boldsymbol{C_2 = \frac{3(B_0^{'}-3)}{2}}$

A slope changes around 2.5 GPa is prominent from this EOS. This proves the existence of an ETT from P-V data. Our observation is consistent with the previous reports on Sb_2Te_3 and Bi_2Te_3[196].

To shed light on the electronic changes under pressure we monitored the relative % changes in lattice parameters and volume under pressure. The lattice parameter c decreases 5.53% whereas a reduces 4.68% in α phase. It interprets the fact that the system is more

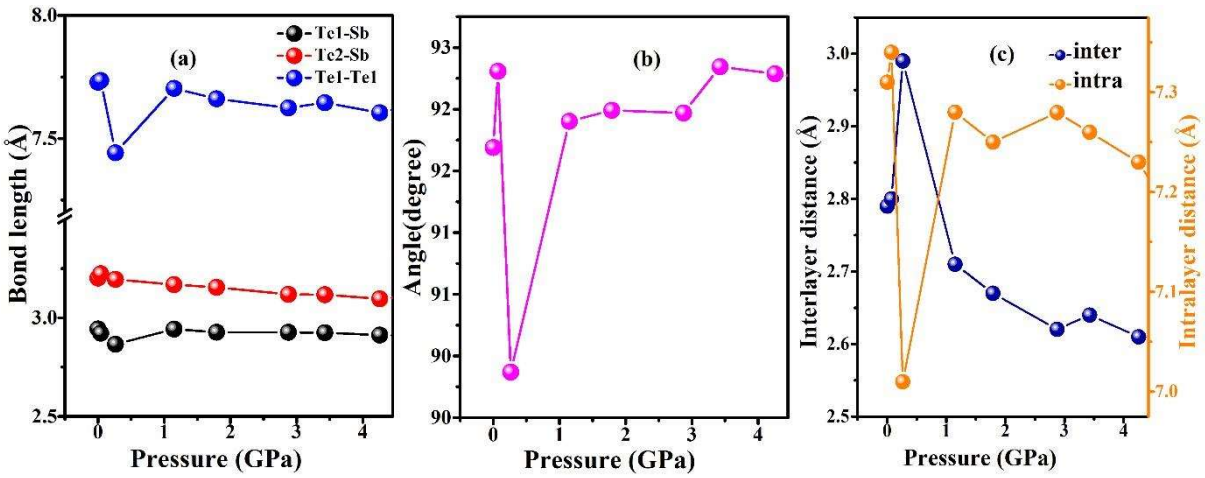

Figure 4.A.4 (a) bond length of Te2-Sb, Te1-Sb and Te2-Te2 as a function of pressure, (b) angle of succession Te1-Sb-Te2 vs pressure, (c) vertical distance between intra-layer and interlayer.

compressible along the c-axis which is not unexpected because of the fact that Sb_2Te_3 has natural tendency of forming layered structure along this axis. The relative decrease in volume is found to be 5.66%, 6.67%, 51.98% for the phase transitions of $\alpha \rightarrow \beta$, $\beta \rightarrow \gamma$ and $\gamma \rightarrow \delta$ respectively. The parent material undergoes 2%, 5%, and 5% volume drops at the phase transitions of 8.0, 13.2, and 21.6 GPa[107]. As mentioned by the report of [217], those values were 3.3%, 2.8%, and 3.8% for the phase transitions of I→II, II→III, and III→IV, respectively. Our sequences of phase transitions are also found in line with other previous ADXRD reports on Sb_2Te_3[107], [186], [193].

In order to relate the electronic transitions stimulated by pressure we have further investigated the bond length, angle and distance inside a quintuple as well as in between two quintuples. We already know that the ambient structure of $Sb_{1.9}Cu_{0.1}Te_3$ is made of quintuple layers (5 atomic layers are covalently bonded). The quintuple layers and atoms in layers are marked as Q1, Q2, Q3, Q4 and A1, A2, A3, A4, A5 respectively displayed in the Figure 4.A.5.

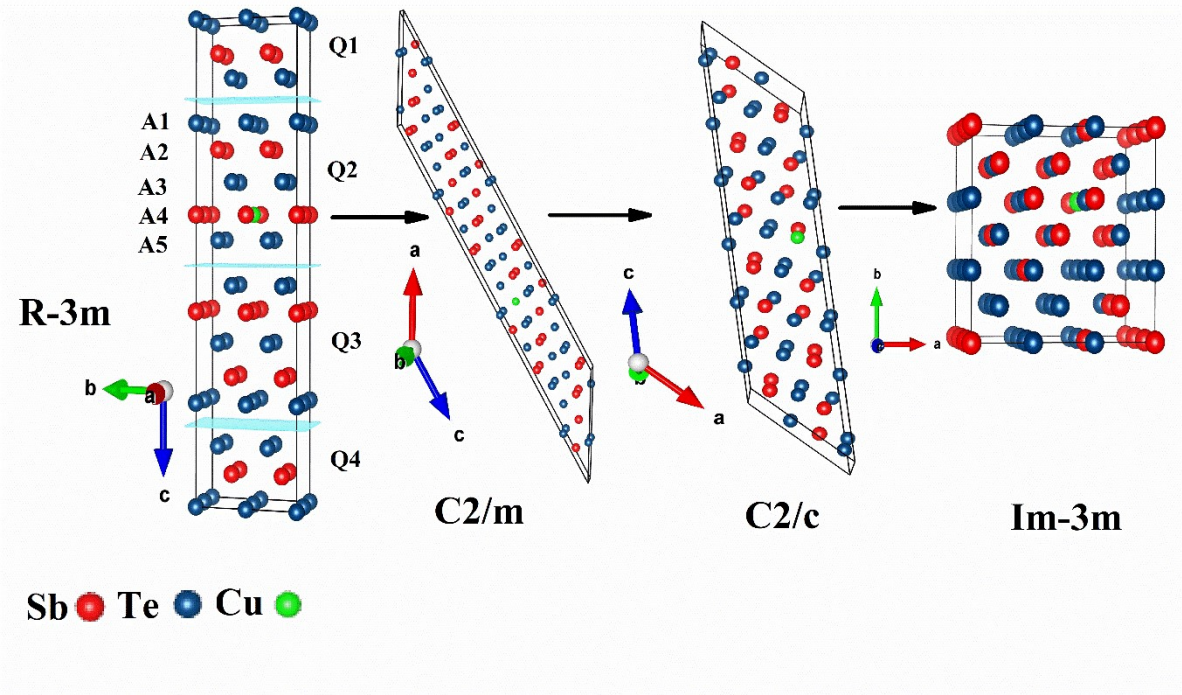

Figure 4.A.5 Schematic of $Sb_{1.9}Cu_{0.1}Te_3$ at various phases I (R-3m), II (C2/m), III (C2/c), and IV (Im-3m) with pressure.

In order to get an insight into the pressure induced electronic transition in phase I, we investigated the changes in angle of succession (Te1(A1)-Sb(A2)-Te2(A3) of Q2), vertical intralayer as well as interlayer distances which are shown in Fig. 3b and Fig. 3c, respectively. We have also explored bond lengths between Te2(A1) of Q2-Te2(A5) of Q2, Te2(A1) of Q2-Sb(A2) of Q2, Te1(A3) of Q2-Sb(A2) of Q2 within the same quintuple layer. The pressure effect on interlayer (Te2 of Q2 and Te2 of Q3) is found to be more evident than other intralayer distances due to stronger pressure effects on vdW bonding (Te2-Te2) over covalent ionic bonding (Te2-Sb and Te1-Sb). The reduction in distance within a quintuple layer as well as in the bond lengths signify that the atoms are coming closer by contraction. The decrease in the spacing between quintuple layers can enhance the coupling between Te and Sb atoms[224], which can also result in the closing of the band gap (DFT results). So, there is a strong possibility of overlapping of atomic orbitals (hybridization) with doping of Cu.

The bond distances of Te2-Te2, Te1-Sb and Te2-Sb vs pressure are shown in Fig. 3a. These bond lengths Te2-Te2, Te1-Sb and Te2-Sb reduces 3.7%, 0.22% and 2.63% respectively from ambient to 0.26 GPa. Te2-Te2 bond length shows a minimum below 1 GPa, then increase and finally slightly reduces around 2 GPa. Under compression a minimum ~ 89.87° is found to be near 1 GPa in angle which stimulates the first electronic transition. A semiconducting to metal transition was also observed at 2 GPa below ETT pressure (4.25 GPa) for the parent compound Sb_2Te_3[207] from theoretical calculation. On further compression, the angle is found to be reducing again at 2 GPa (Figure 4.A.4b). This change can be described as ETT. This trend is similar to the result obtained by S. M. Souza et al[193]. All the figures (Figure 4.A.4 a, b, c) show first minimum at semiconductor-metal transition (discussed later in details) under pressure followed by a second minimum at ETT. Thus, we can say that pressure-induced ordering inside QLs has significant contribution on the first electronic transition that is occurring at a pressure less than 1 GPa.

4.A.3.2 Raman measurement In order to corroborate the structural transitions found from XRD we further performed Raman experiment. The anomaly in the two new Raman modes and their distinct slope changes validate our previous assumption on electronic transitions. High pressure Raman spectra of Cu doped Sb_2Te_3 is recorded up to 30 GPa and is shown in Figure 4.A.6a and b. The α-phase is a centrosymmetric structure that contains a primitive cell with Sb and one Te atoms occupying 6c Wycoff positions and remaining one Te atom located at 3a Wyckoff site. Therefore, group theory allows total 10 zone-center modes, which can be represented as following[225]:

$$\boldsymbol{\Gamma_{10} = 2A_{1g} + 3A_{2u} + 2E_g + 3E_u} \qquad \textbf{(4.A.3)}$$

The two acoustic branches are A_{2u} and doubly degenerated E_u mode, while the rest correspond to optic modes. Gerade (g) modes are Raman active while ungerade (u) modes are infrared (IR) active. Hence, there are four Raman-active modes ($2A_{1g} + 2E_g$) and four

IR-active modes ($2A_{2u} + 2E_u$). The E_g modes correspond to in plane vibrations, while the A_{1g} modes represent out of plane vibrations along the c axis.

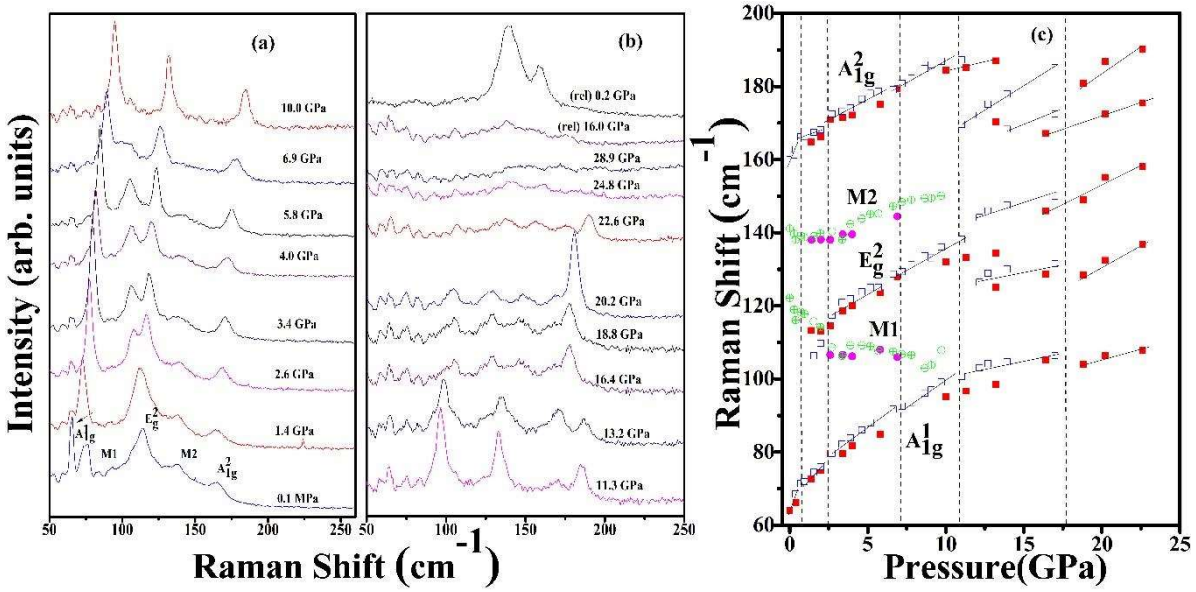

Figure 4.A.6 Experimental Raman spectra of $Sb_{1.9}Cu_{0.1}Te_3$ at pressures (a) 0.1 MPa - 10 GPa, (b) 11.3 - 30 GPa, (c) Pressure dependence of the Raman frequencies, the vertical dashed lines are an estimation of the pressure at which the electronic and structural phase transitions occur, blue hollow square and green crossed circles are for one run, red solid squares and magenta solid circles are for another run of Raman measurements.

Raman spectra at ambient pressure (outside the DAC) show three Raman modes: A^1_{1g} at ~ 65 cm^{-1}, E_g^2 at ~113 cm^{-1}, and A^2_{1g} at ~165 cm^{-1}, which is in good agreement with earlier reported work on bulk Sb_2Te_3[207] as well as few other quintuples[185], [186], [226]. We could not observed E_g^1 mode (40 cm^{-1}) due to the spectral width of filter[185]. Two new Raman modes were observed M1 at 122 cm^{-1} and M2 at 140 cm^{-1} which are basically infrared active modes. The odd-parity IR active phonon modes are Raman forbidden and do not appear in the Raman spectrum for bulk crystals with crystal symmetry. These modes are interesting to discuss here in details. These modes are similar to the P1 and P2 modes observed in Sb_2Te_3/Ge heterostructures[227]. Singh group[228] assigned the former mode as A_{2u}~ 115 cm^{-1} and the later one as A^3_{2u}~144 cm^{-1}. Those IR-active modes also appear as Raman mode in pristine Bi_2Te_3[229]–[232] as a result of crystal symmetry breaking due to

the presence of two interfaces (top and bottom). Similar IR-active vibrational modes appear as Raman mode as a result of local crystal symmetry breaking by the In- diffusion in Bi_2Se_3[233] and in pristine Bi_2Se_3[234]. In the present study, M1 mode softens up to 3.5 GPa whereas M2 mode softens up to 1.4 GPa, with further compression both of them shows a stiffening trend. The softening trend at the low pressure is identical to that of A_{1g} at 140 cm^{-1} and E_g at 122 cm^{-1} modes in 1T-$TiTe_2$ single crystal under pressure[235]. In general, the phonon modes are expected to stiffen (blue shift) during the hydrostatic lattice compression. All the Raman active modes except M1 and M2 show an increase in frequency with increasing pressure (Figure 4.A.6c) is in good agreement with previous reports on Sb_2Te_3[185] for the rhombohedral phase[185], [186], [193]. The observed Raman results are reproducible in multiple runs. These outcomes are also in agreement with the reports on Bi_2Te_3 and Bi_2Se_3[186]. But, Fig. 4c shows that the behavior of these two modes is anomalous and we can identify two distinct pressure regions. Importantly, softening as well as changing in slope of Raman frequencies are usually associated with electronic transitions[203], [236]. These two Infrared active modes appear as Raman modes are possibly because of symmetry breaking arising due to disorder produced by Cu in Sb_2Te_3. Similar behavior was observed in Se doped Bi_2Te_3[237].

The α-phase transform to β-phase under pressure at 8 GPa. Group theory predicts 30 vibrational modes for the C2/m phase of parent sample Sb_2Te_3 with the following representations-

$$\boldsymbol{\Gamma_{30} = (10A_g + 10B_u) + (5B_g + 5A_u)} \qquad \textbf{(4.A.4)}$$

Among them one A_u and two B_u are the acoustic phonons, and the rest are optical phonons. However, one can expect 15 zone-centre Raman-active ($10A_g + 5B_g$) modes for the C2/m phase. Due to higher signal-noise ratio we could follow the 3 Raman modes only. Again,

under pressure β phase transform to γ-phase at 11.3 GPa and for the C2/c phase, from the group theory-

$$\Gamma_{30} = (7A_g + 7A_u) + (8B_g + 8B_u) \quad (4.A.5)$$

All are optical modes except A_u and B_u, so there are 15 zone-centre Raman active modes for this particular phase. Our system finally undergoes to a disordered cubic phase above 17.5 GPa. We have identified a lack of Raman signal above 22 GPa, thus suggesting Raman-inactive phase above that pressure. Raman data suggests a complete phase transition towards δ-phase which is the disordered bcc structure with Im-3m space group which is similar as found in other TIs[107], [217], [238].

4.A.3.3 Theoretical discussions To investigate the origin corresponding to electronic changes, we performed *ab-initio* theoretical calculations (Figure 4.A.7a-c and 4.A.8a-c) on

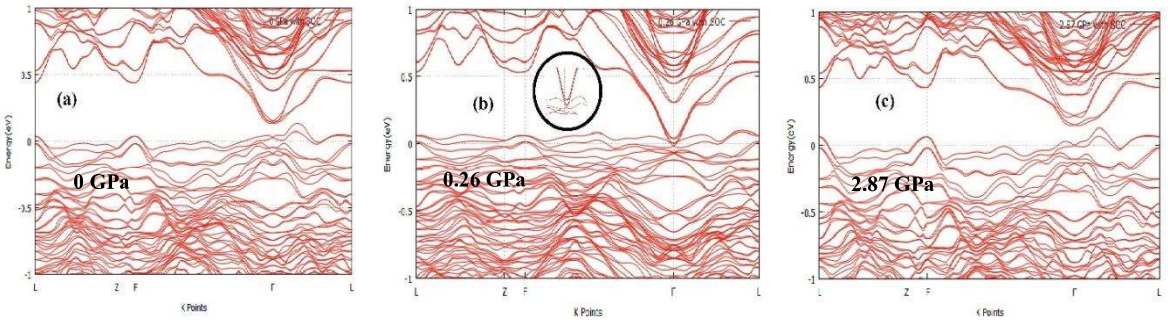

Figure 4.A.7 (a) Bulk bandstructure of $Sb_{1.9}Cu_{0.1}Te_3$ at 0 GPa, (b) 0.26 GPa;inset: magnifying view at Γ-point shown, (c) 2.87 GPa. The Fermi level is set to zero.

α-phase. The band structure of Figure 4.A.7a depicts semiconducting behaviour (zero density of states value at the Fermi level Figure 4.A.8a) at 0 GPa. Interestingly, we can see the conduction band to (Figure 4.A.7b) pass through the valence band very closely for a pressure 0.26 GPa. The closure in bulk conduction band minima and valence band maxima indicates the semiconductor to metal transition with regards to band topology. This proves that the first electronic transition we observed is actually a semiconductor to metal

transition. Moreover, at pressure 2.87 GPa above ETT (2 GP), the topology of the Fermi surface is found to be changed. The band gap between conduction band minima (CBM) and valence band maxima (VBM) is found to be reduced around Z point but it is enhanced at high symmetry Γ-point (shown in Figure 4.A.7c) compared to ambient pressure (Figure 4.A.7a). This observation is similar as reported in Sb_2Te_3[189] and Bi_2Te_3[190].

Importantly, the zero DOS at the Fermi level signifies semiconducting character at the ambient pressure, shown in Figure 4.A.8a. As the pressure increases to 0.26 GPa, finite density of states at the Fermi level indicating metallic character for 0.26 GPa condition. From the DOS Figure 4.A.8b, we can also notice the Cu-*3d* states to significantly overlap with the Te 5p states near the Fermi level, suggesting a *p-d* hybridization between them and results in such a metallic transition. In the ambient conditions, we have already noticed strong hybridization between Cu-*d* state, Sb- *p* state and Te-*p* state [239]. The replacement of Cu however increases the band overlapping or mixing of Te-*p* and Cu-d states. We observe that the pressure-induced change of lattice parameters should become the leading role for the overall band-gap closing situation. Moreover, it is the copper which enhance the possibility of hybridization. The band gap of Cu-doped Sb_2Te_3 is 0.082 eV (DOS) without pressure which is comparatively less than that of the pristine Sb_2Te_3[240]. The strong hybridization between Cu and Te atoms will cause the overlap of bands under pressure, which leads to the closure of band gap. This is similar to Cr doped Sb_2Te_3[224]. To authenticate our justification of Cu behind the metallic transition we calculated the bandstructure (not shown) with same lattice parameters and wychoff position obtained at 0.26 GPa without introducing any Cu atom into the system. Interestingly, we see no such band closing event to occur at that pressure.

For the calculation, tuning of Fermi level was done by introducing excess electrons to balance the hole doping. Similar Fermi level shifting was also noticed in Mn doped Bi_2Te_3

and manipulated with electron doping[241], [242]. One can also create Te vacancy to compensate hole doping, in that case removing Te and substitution of Cu at Sb site should be from the same quintuple[241].

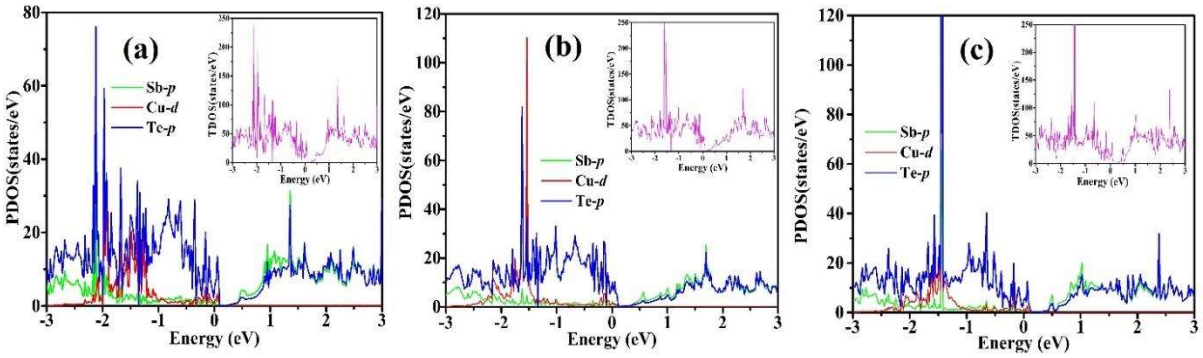

Figure 4.A.8 Projected DOS and inset: Total DOS at (a) 0 GPa, (b) 0.26 GPa and (c) 2.87 GPa. The Fermi level is set to zero.

4.A.4 Conclusions

We have grown the single crystal topological insulator $Sb_{1.9}Cu_{0.1}Te_3$, and performed combined study of synchrotron XRD and Raman up to 32 GPa. Further, we portray the detail vibrational, structural and electrical picture of this compound under high pressure. We have provided evidences for the observation of two electronic transitions and three structural transitions from ambient R-3m to monoclinic C2/m to another monoclinic C2/c and finally into a bcc Im-3m phase. The characterization of structural part depicts the presence of structural transitions at 8.28, 12.75 and 16.77 GPa respectively with appearance of various newly diffraction peaks. The lattice parameters ratio c/a anomaly as a function of pressure together with discontinuous compressibility data unveil the presence of an electronic topological transition because of the changes in topology of the Fermi surfaces at a lower pressure compared to the parent materials. The experimental observation of semiconductor to metal transition due to closure of bulk band gap is confirmed by our theoretical *ab-initio* calculations. The electronic overlapping induced by Cu under the pressure stimulates the metal transition and the transition pressure is lowest among the A_2B_3

TI family. Raman frequency anomaly up to 3 GPa strengthen our former observations. Hence our comprehensive studies on $Sb_{1.9}Cu_{0.1}Te_3$ opens up new opportunity for the investigation of metallization property under pressure.

B. Pressure induced topological and structural transitions in iron and sulphur doped Sb_2Te_3

4.B.1 Introduction

Topological insulators (TI) have revolutionized recent condensed matter physics with their time reversal symmetry protected surface states[243] that reside inside the bulk band gap. Besides that, pressure-induced electronic topological transition (ETT) or isostructural phase transition (IPT)[244], topological superconductivities[189] and substitutional alloy formation[217], [238] provoked significant research interests in the field of TIs. ETT or Lifshitz transition is an isostructural transition that does not bring any volume discontinuity and change in Wyckoff positions of atoms with pressure. It has been observed that many of these topological insulators undergo several structural phase transitions and ultimately forming a cubic phase at high pressure. In addition, Fermi surface modification also leads to an ETT in these family of compounds. Our earlier studies indicate that doping affects the pressure of transformation in these layered topological insulators[245]. In order to further understand the effect of doping on the pressure of transformations we have now carried out high pressure angle dispersive x-ray diffraction studies on these compounds.

4.B.2 Results and discussion

The refinement of the ambient phase shows that $Sb_{1.9}Fe_{0.1}S_{0.15}Te_{2.85}$ can be fitted with the R-3m space group 166 and the lattice constants were found to be $\boldsymbol{a} = \boldsymbol{b} = 4.25905$ Å, $\boldsymbol{c} = 30.44409$ Å. Doping of Fe and S in Sb_2Te_3 shows a reduction in the lattice parameters, which could be due to the smaller atomic radii of Fe (1.26 Å) and S (1.09 Å) compared to Sb (1.45 Å) and Te (1.40 Å). The ambient structure can be described as a stacking of 5 layered blocks along the ***c***-axis linked by van der Waals forces. These blocks, called as quintuple layers [246] (Figure 4.B.1a), are formed of alternating layers of Sb and Te in the order of Te1–Sb–Te2–Sb–Te1. Figure 4.B.2b expresses single crystal XRD of the material.

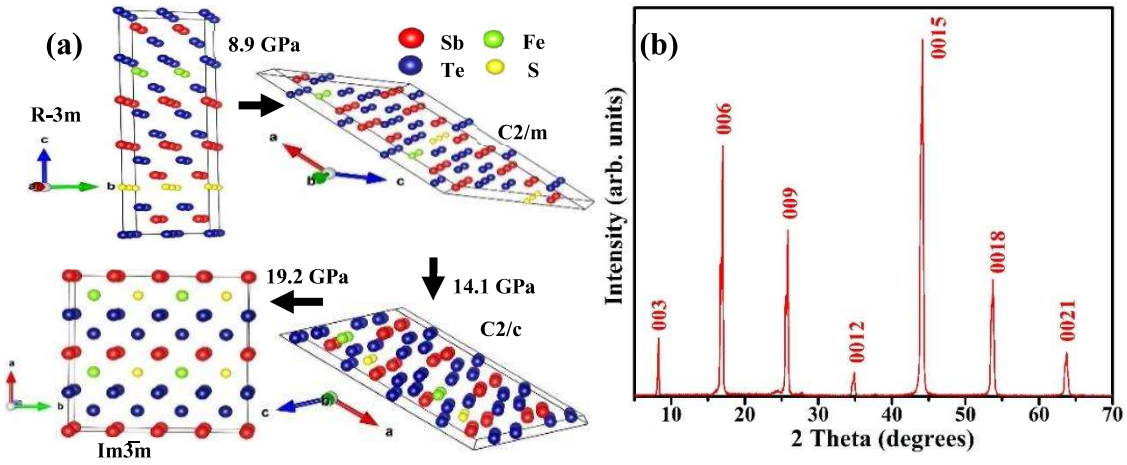

Figure 4.B.1 Schematics of $Sb_{1.9}Fe_{0.1}S_{0.15}Te_{2.85}$ structures at different pressures: (a) ambient R-3m, C2/m above 8.9 GPa, C2/c above 14.1 GPa, and $Im\bar{3}m$ above 15.1 GPa, (b) Single crystal XRD of $Sb_{1.9}Fe_{0.1}S_{0.15}Te_{2.85}$.

High pressure ADXRD data of $Sb_{1.9}Fe_{0.1}S_{0.15}Te_{2.85}$ at few representative pressures has been shown in Figure 4.B.2a. Under pressure, $Sb_{1.9}Fe_{0.1}S_{0.15}Te_{2.85}$ undergoes three structural phase transitions. It can be seen that there is a considerable overlap of the different structural phases at high pressure. Inspection of the diffraction peaks of the new high pressure phases shows that, though the transformation pressure is different, the sequence of phase transition is similar to pure TIs [244], [247], [248].

The lattice parameters of all the phases were determined by carrying out Rietveld analysis. We observed the transformation of ambient R-3m (phase I) to the C2/m (phase II) at ~8.9 GPa. Phase I coexists with phase II up to 10.75 GPa. Appearance of new diffraction peaks marked with a * indicate the transformation to a new phase C2/c (phase II) at 14.1 GPa. Both the C2/m (phase II) and C2/c (phase III) phases coexist between 14.1 -16.8GPa. On further increasing the pressure, phase III transforms to a disordered cubic phase $Im\bar{3}m$ (phase IV) at 19.2 GPa and coexistence of phase III and phase IV is observed across 19.2 - 23.5 GPa. The phase IV diffraction peaks can be indexed to a disordered **bcc** structure

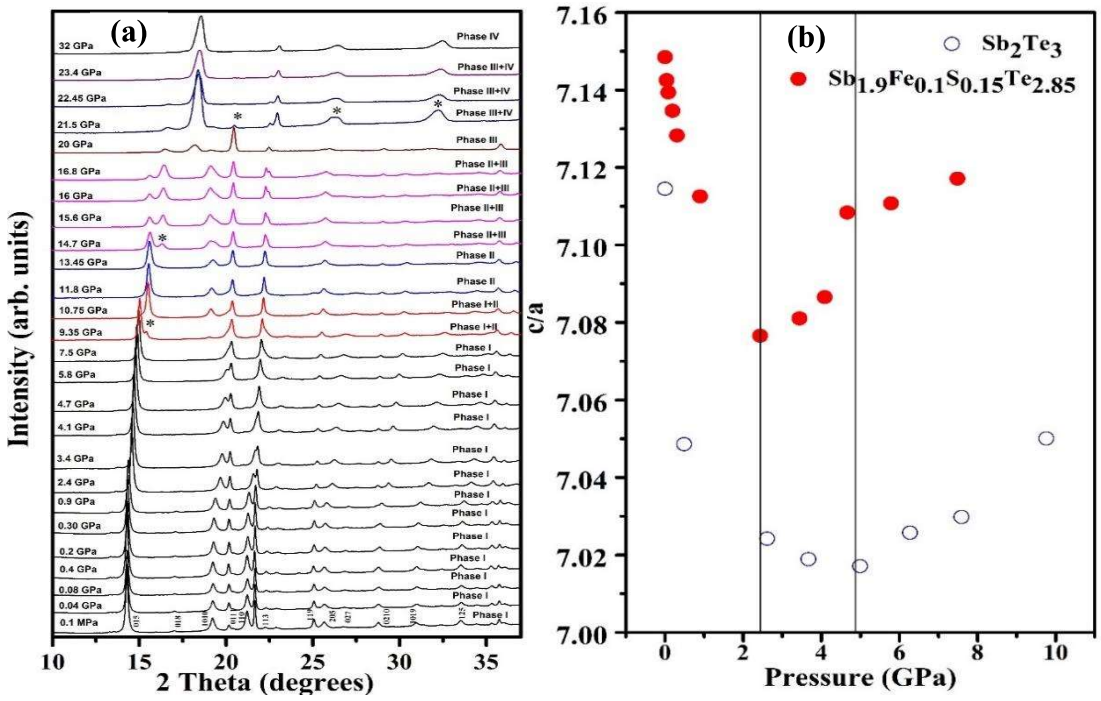

Figure 4.B.2 (a) ADXRD of $Sb_{1.9}Fe_{0.1}S_{0.15}Te_{2.85}$ up to 32 GPa, (b) c/a anomaly with pressure: solid red circles show c/a anomaly with pressure, hollow circles show comparison with pure Sb_2Te_3 Souza *et al* [193].

which is stable beyond 19.2 GPa. Within the $Im\bar{3}m$ phase, the Sb, Te, Fe and S atoms are found to be randomly distributed on the bcc lattice sites. The fourth phase is found to be stable up to 32 GPa. On release of pressure, the ambient phase is retrieved.

Pressure vs volume is plotted for each structural phase and is shown in Figure 4.B.3a. Figure 4.B.3c shows the fit of the PV data to the Birch Murnaghan equation of state which is given below-

$$\mathbf{P(V)} = \frac{3}{2}\mathbf{B_0}[(\frac{\mathbf{V_0}}{\mathbf{V}})^{\frac{7}{3}} - (\frac{\mathbf{V_0}}{\mathbf{V}})^{\frac{5}{3}}] \times \{\mathbf{1} + \frac{3}{4}(\mathbf{B_0^{'}} - \mathbf{4})[(\frac{\mathbf{V_0}}{\mathbf{V}})^{\frac{2}{3}} - \mathbf{1}]\} \qquad \textbf{(4.B.1)}$$

The extracted bulk modulus and its derivative for the rhombohedral phase is listed in Table 4.B.1. The values agree well with previous reports on Sb_2Te_3[193], [196]. This indicates that doping does not affect the mechanical properties of this topological insulator.

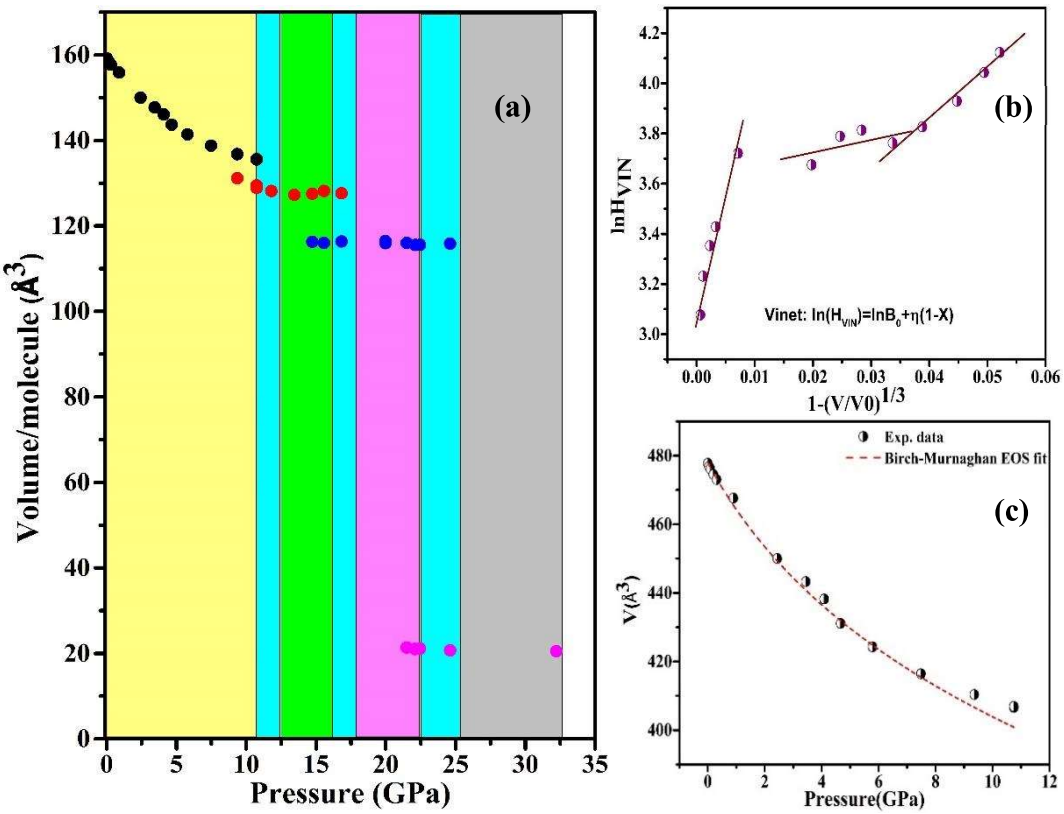

Figure 4.B.3 (a) Volume as a function of pressure for all 4 phases, (b) Universal equation of state ln H as a function of 1-X, (c) Fitting of 3rd order Birch-Murnaghan EOS on rhombohedral phase.

The PV curve of the first phase does not show any discontinuity. However, since the Universal Equation of State (UEOS) [249] can give signatures of the presence of an electronic transition we transformed the equation of state to the Universal Equation of State (UEOS). The UEOS is proposed by Vinet and given by-

$$\boldsymbol{lnH_{VIN} = lnB_o + \eta(1 - X)} \qquad \textbf{(4.B.2)}$$

Where $\boldsymbol{H = PX^2/3(1 - X)}$ and $\boldsymbol{X = (V/Vo)^{1/3}}$, η being related to the pressure derivative (B'_o) of the bulk modulus B_o, $\boldsymbol{\eta = 3(B'_o - 1)/2}$ and V is the volume at pressure P and V_0 is the ambient volume. As shown in Figure 4.B.3b a discontinuity is observed indicating the presence of an electronic change as a function of pressure.

In fact, the plot of the ***c/a*** ratio vs pressure of the rhombohedral phase shows minima at ~2.5 GPa (Figure 4.B.2b). This change in the slope of the c/a ratio, ie. the presence of a minima is attributed to the presence of an ETT.

Table 4.B.1 The lattice parameters and angles for different phases. Bulk modulus and its derivative are also depicted for initial phase.

Phases	Lattice Constant (Å)
R-3m (166)	$\boldsymbol{a}$ = 4.2592 $\boldsymbol{c}$=30.4474 at 0 GPa $\boldsymbol{B_0}$ = 30.67 GPa $\boldsymbol{B_0'}$ = 8.29
C2/m (12)	$\boldsymbol{a}$ = 14.5512 $\boldsymbol{b}$ = 4.0962 $\boldsymbol{c}$ = 17.1921 β = 149.2126 at 9.3 GPa
C2/c (15)	$\boldsymbol{a}$ = 9.4268 $\boldsymbol{b}$ = 6.9041 $\boldsymbol{c}$ = 10.04427 $\boldsymbol{\beta}$ =134.6438 at 14.7 GPa
$Im\bar{3}m$ (229)	$\boldsymbol{a}$ = 3.49888 at 21.5 GPa

ETT or Lifshitz transition occurs when band extrema associated with van Hove singularity passes through the Fermi level and causes distribution of carriers. This electronic topological transition is recorded at lower pressures when compared to pure Sb_2Te_3 (~3 GPa)[193]. It shows that doping by lower atomic radii atoms reduces the ETT threshold pressure.

The phase-transition pressure of ~9.3 GPa for Sb_2Te_3 is larger than that of Bi_2Te_3 (~8.2 GPa), which might be caused by the smaller atomic radii of the Sb to Bi atoms. However, further doping of smaller radii atoms of Fe and S does not increase the transition pressure but decreases it to ~8.9 GPa.

Second structural transition from monoclinic (C2/m) to monoclinic (C2/c) phase is observed at 14.1 GPa. In Bi_2Te_3 and Sb_2Te_3 the second phase transition was observed at 13.4 and 15.1 GPa. However, in Sb_2Te_3 it was observed that the new phase is a disordered C2/m phase unlike Bi_2Te_3 where this structure is similar to C2/c. Formation of this disordered C2/m structure has been attributed to comparable atomic radii of Sb and Te[217]. However, in Bi_2Te_3 where atomic radii of Bi and Te differ substantially, the disordered structure was not observed[238]. The atomic radii of iron and Sulphur are substantially different from Sb and Te, but the compound $Sb_{1.9}Fe_{0.1}S_{0.15}Te_{2.85}$ does not form a disordered monoclinic (C2/m) structure like its parent Sb_2Te_3 but transforms to a new monoclinic structure C2/c. Third structural transition from C2/c to $Im\bar{3}m$ phase is observed at 19.2 GPa. However, in Sb_2Te_3 and Bi_2Te_3 this phase transition was observed at 19.8 GPa and 14.4 respectively. These transition shows that as pressure is increased, atomic radii of iron and Sulphur do not drastically affect the pressure of formation of the disordered cubic phase.

4.B.3 Conclusions

High pressure studies of $Sb_{1.9}Fe_{0.1}S_{0.15}Te_{2.85}$ show ETT at ~ 2.5 GPa and structural phase transition at ~ 8.9 GPa, ~ 14.1 GPa and ~19.2 GPa. It is to be noted that atomic radii of doped constituent atoms in Sb_2Te_3 drastically affects the ETT. However, its effect on structural phase transitions is not found to be very large. Instead of forming disordered monoclinic (C2/m) structure $Sb_{1.9}Fe_{0.1}S_{0.15}Te_{2.85}$ transforms to new monoclinic structure C2/c and subsequent structural transitions are observed at similar pressure range. Our studies show that doping lowers the pressure of transformation of the high pressure disordered cubic phase. These studies indicate that appropriate doping can indeed help us to trap unique states at ambient pressure and can thus help in synthesizing new materials.